JOURNAL OF GUIDANCE, CONTROL, AND DYNAMICS
Vol. 21, No. 3, May–June 1998

Maneuvering Flight Control

M. Pachter*
U.S. Air Force Institute of Technology, Wright–Patterson Air Force Base, Ohio 45433-7765
and
P. R. Chandler† and L. Smith‡
U.S. Air Force Research Laboratory, Wright–Patterson Air Force Base, Ohio 45433-7531

The development of control laws for maneuvering flight, specifically, a high-amplitude velocity vector roll, is addressed. The plant model has seventh-order nonlinear dynamics with coupled pitch and lateral directional dynamics. Using time scale separation and pointwise linearization about nonequilibria trajectories, a receding horizon linear quadratic optimal control law with full state feedback is synthesized on-line. Also on-line, the pilot inputs are modified using linear programming to prevent actuator rate saturation over the optimization horizon. The nonlinear control law performance is demonstrated in a fighter aircraft simulation with a rudder failure during a loaded roll maneuver. The performance of the controller during aggressive pitch and yaw maneuvers is also demonstrated. The work described in this paper is confined to model-based receding horizon optimal control law synthesis; one will rely on on-line system identification to provide the failed aerodynamic stability and control derivatives, thus achieving indirect adaptive control.

I. Introduction

A GENERIC three-channel nonlinear flight control system for high-amplitude maneuvers is designed, with special reference to the velocity vector, or stability axis, roll maneuver. During a velocity vector roll, the aircraft rotates about an axis aligned with its velocity vector. This maneuver is also an element of the close air combat *S* maneuver, where one would like to roll the loaded airframe, rather than first unload, roll, and pull *g*s.

Perhaps the most significant difficulty in designing a controller for a fast velocity vector roll is accounting for the nonlinearities introduced into the system by the maneuver itself. The high-amplitude velocity vector roll maneuver invalidates, in part, the small perturbations hypothesis that lies at the heart of linearization. Thus, these kinematic nonlinearities must be included in the aircraft model that is used in the velocity vector roll control system design. Therefore, standard linear aircraft models and standard linear flight control system design techniques such as separation of the longitudinal and lateral/directional control channels cannot be used.

The objective of this work is to design a high-amplitude velocity vector roll controller with minimal cross coupling, even during failures. This paper is a sequel to the work[1,2] where the plant model was established, a timescale separation argument was evoked (see also Ref. 3), and a linearized control system was analyzed. In addition, a linear quadratic optimal control law that used full state feedback was synthesized and used in a receding horizon tracking control scheme. In this paper, pointwise linearization at every Δt about nonequilibria trajectories is employed, which is suitable for nonlinear flight control. Total, rather than perturbation, variables are used. In addition, a linear programming (LP) module is included in an outer-loop type of arrangement to modify the pilot's inputs such that the surface deflection commands will not cause actuator rate saturation for any surface over the planning horizon. The work described is confined to model-based receding horizon optimal control law synthesis; one will rely on on-line system identification to provide the failed aerodynamic stability and control derivatives, thus achieving indirect adaptive control. This plan of action has been carried through for the pitch channel in Ref. 4. Also, the on-line identification of all of the aircraft stability and control derivatives, including the lateral directional stability and control derivatives, is presented in Ref. 5, where the full mechanization of indirect adaptive control is accomplished.

The paper is organized as follows. In Sec. II, the nonlinear dynamics pertinent for velocity vector roll control are given. A pointwise linearization scheme for the fast dynamics is developed in Sec. III, and a full state feedback linear quadratic optimal control formulation with linear programming is presented in Sec. IV. The performance of the proposed nonlinear flight control system is shown in Sec. V when, at 1 s into a loaded roll, the aircraft is subject to a 50% rudder loss. The performance of the controller during aggressive pitch and yaw maneuvers is also demonstrated. Concluding remarks are made in Sec. VI.

II. Nonlinear Dynamics

The seven states are $P, Q, R, V/\bar{U}, W/\bar{U}, \theta$, and ϕ. The following definitions for the aerodynamic angles are used (see, for example, Ref. 6, p. 141):

$$\alpha = A\tan(W/\bar{U}), \qquad \beta = A\tan(V/\bar{U})$$

The aerodynamic database[7] is used to generate constant linear stability and control derivatives for a 3-*g* level turn in the heart of the envelope at 10,000 ft and $M = 0.7$. Using the constant U hypothesis and stability axes, the following nonlinear dynamics are obtained (see, for example, Ref. 8):

$$\frac{\mathrm{d}}{\mathrm{d}t}\left(\frac{V}{\bar{U}}\right) = \left(\frac{W}{\bar{U}}\right)P + \left(C_{y_r} - 1\right)R + \frac{g}{\bar{U}}\sin\phi\cos\theta + C_{y_p}P + C_{y_\beta}\beta + C_{y_{\delta_r}}\delta_r, \qquad 0 \le t, \qquad V(0) = V_0 \tag{1}$$

$$\frac{\mathrm{d}}{\mathrm{d}t}\left(\frac{W}{\bar{U}}\right) = \left(1 + C_{z_q}\right)Q - \left(\frac{V}{\bar{U}}\right)P + \frac{g}{\bar{U}}\cos\phi\cos\theta + C_T\sin\left(\alpha^s_{0L} - \alpha^b_{0L}\right) - C_{z_\alpha}\alpha_{0L} + C_{z_\alpha}\alpha + C_{z_{\dot\alpha}}\dot\alpha + C_{z_{\delta_e}}\delta_e \qquad W(0) = W_0 \tag{2}$$

$$\frac{\mathrm{d}P}{\mathrm{d}t} = C_{l_{pq}}PQ + C_{l_{qr}}QR + C_{l_p}P + C_{l_r}R + C_{l_\beta}\beta + C_{l_{\delta_a}}\delta_a + C_{l_{\delta_r}}\delta_r, \qquad P(0) = P_0 \tag{3}$$

$$\frac{\mathrm{d}Q}{\mathrm{d}t} = C_{m_{pr}}PR + C_{m_{p^2}}R^2 - C_{m_{p^2}}P^2 + C_{m_0} + C_{m_\alpha}\alpha + C_{m_{\dot\alpha}}\dot\alpha + C_{m_q}Q + C_{m_\delta}\delta_e - C_{m_T}, \qquad Q(0) = Q_0 \tag{4}$$

Received June 26, 1997; revision received Oct. 20, 1997; accepted for publication Nov. 26, 1997. This paper is declared a work of the U.S. Government and is not subject to copyright protection in the United States.

*Professor, Department of Electrical and Computer Engineering. Member AIAA.
†Senior Flight Control Scientist, Flight Control Division. Member AIAA.
‡Captain, Aerospace Engineer, Flight Control Division.

$$\frac{dR}{dt} = C_{n_{pq}} PQ - C_{l_{pq}} QR + C_{n_p} P + C_{n_r} R + C_{n_\beta}\beta + C_{n_{\delta_a}}\delta_a + C_{n_{\delta_r}}\delta_r, \qquad R(0) = R_0 \tag{5}$$

where the parameters

$$C_{m_T} = (\Delta z_{CG}/I_y)T[1/s^2], \qquad C_T = T/m\bar{U}[1/s]$$

and T is thrust. The stability axes are chosen so that, at the inception of the velocity vector roll maneuver at time $t = 0$, then $W_0 = 0$, $\alpha_0 = 0$, and $\theta_0 = 0$. These axes are maintained throughout the duration of the maneuver. This convention is adopted throughout. The θ and ϕ Euler angles, Eqs. (6) and (7), are needed to resolve the force of gravity into the body axes:

$$\dot{\theta} = Q\cos\phi - R\sin\phi, \qquad \theta(0) = \theta_0, \qquad \theta(t_f) = \theta_f \tag{6}$$

$$\dot{\phi} = P + Q\sin\phi\tan\theta + R\cos\phi\tan\theta \qquad \phi(0) = \phi_0, \qquad \phi(t_f) = \phi_f \tag{7}$$

III. Pointwise Linearization and Time Scale Separation

In this work, linearization about arbitrary, nonequilibria trajectories is performed. This concept is used in a receding horizon linear quadratic (LQ) optimal tracking control scheme. Minimal modeling error is accrued in this approach, which is beneficial in adaptive and reconfigurable control design, as well as system identification. In addition, the pointwise linearization approach obviates the need for considering nonlinear time-invariant nominal dynamics.

The pointwise linearization approach is now developed and applied to the nonlinear dynamics of flight control. The nonlinear plant is linearized at the current time t, and the linearized dynamics are used over the model predictive control horizon. The linearization is repeated at each sampling interval Δt. Thus, the nonlinear control system is

$$\dot{X} = f(X, U)$$

The window $t \le \tau \le t + T$ is considered, where T is the optimization horizon. At time t

$$X(t) = X_0$$

where the subscript 0 merely denotes the state at which the linearization is performed; it does not indicate a trim condition. From the linear aerodynamics hypothesis it follows that

$$\dot{X} = f(X) + \tilde{B}U$$

Now,

$$f(X) \approx f(X_0) + f_X|_{X_0}(X - X_0) = f_X|_{X_0} X + [f(X_0) - f_X|_{X_0} X_0]$$

approximately holds, provided that X is close to X_0. Hence,

$$\dot{X} = f_X|_{X_0} X + \tilde{B}U + [f(X_0) - f_X|_{X_0} X_0]$$

Note that in this linearization method total, not perturbation, variables are used.

Furthermore, partition the state

$$X = \begin{bmatrix} X_1 \\ X_2 \end{bmatrix}, \qquad X_0 = \begin{bmatrix} X_{1_0} \\ X_{2_0} \end{bmatrix}$$

and

$$f = \begin{bmatrix} f_1(X_1, X_2) \\ f_2(X_1, X_2) \end{bmatrix}, \qquad \tilde{B} = \begin{bmatrix} B_1 \\ B_2 \end{bmatrix}$$

Hence,

$$\dot{X}_1 = f_1(X_1, X_2) + B_1 U, \qquad \dot{X}_2 = f_2(X_1, X_2) + B_2 U$$

Suppose that the X_2 components of the state change slowly, viz., $X_2(\tau) \approx X_{2_0}$ for $t \le \tau \le t + T$. Hence,

$$\dot{X}_1 = f_1\left(X_1, X_{2_0}\right) + B_1 U$$

Thus, similar to the earlier analysis,

$$\dot{X}_1 = f_{1_{X_1}}\Big|_{X_{1_0}, X_{2_0}} X_1 + B_1 U + \left[f_1\left(X_{1_0}, X_{2_0}\right) - f_{1_{X_1}}\Big|_{\left(X_{1_0}, X_{2_0}\right)} X_{1_0}\right]$$

Define

$$A = f_{1_{X_1}}\Big|_{\left(X_{1_0}, X_{2_0}\right)}, \qquad B = B_1$$

$$\boldsymbol{c} = f_1\left(X_{1_0}, X_{2_0}\right) - f_{1_{X_1}}\Big|_{\left(X_{1_0}, X_{2_0}\right)} X_{1_0}$$

Hence, for the planning horizon $t \le \tau \le t + T$, the linear system

$$\dot{X}_1 = AX_1 + BU + \boldsymbol{c}$$

is obtained. Using total, rather than perturbation, variables, introduces the intercept $\boldsymbol{c}$. The linear quadratic regulator optimization problem is solved and the optimal control $U^*(\tau)$ is computed. Moreover, the optimal control time history is used to propagate the complete nonlinear system and obtain $X_1(\tau), X_2(\tau), t \le \tau \le t + T$, i.e.,

$$\dot{X}_1 = f_1(X_1, X_2) + B_1 U^*(\tau), \qquad \dot{X}_2 = f_2(X_1, X_2) + B_2 U^*(\tau) \qquad t \le \tau \le t + T$$

In our flight control application, the fast and slow states and the control variables are

$$X_1 = \begin{bmatrix} P \\ Q \\ R \\ \alpha \\ \beta \end{bmatrix}, \qquad X_2 = \begin{bmatrix} \theta \\ \phi \end{bmatrix}, \qquad \text{and} \qquad U = \begin{bmatrix} \delta_e \\ \delta_a \\ \delta_r \end{bmatrix}$$

respectively. In addition, in our flight control application [see Eqs. (1–5)]

$$f_1(X_1, X_2) = f_{11}(X_1) + f_{12}(X_2)$$

where

$$f_{11} = \begin{bmatrix} C_{l_{pq}} PQ + C_{l_{qr}} QR + C_{l_p} P + C_{l_r} R + C_{l_\beta}\beta \\ C_{m_{pr}} PR + C_{m_{p^2}} R^2 - C_{m_{p^2}} P^2 + C_{m_0} + C_{m_\alpha}\alpha + C_{m_{\dot{\alpha}}}\dot{\alpha} + C_{m_q} Q - C_{m_T} \\ C_{n_{pq}} PQ - C_{l_{pq}} QR + C_{n_p} P + C_{n_r} R + C_{n_\beta}\beta \\ \left(1 + C_{z_q}\right)Q - (V/\bar{U})P + C_{z_\alpha}\alpha + C_{z_{\dot{\alpha}}}\dot{\alpha} - C_{z_\alpha}\alpha^s_{0L} + C_T \sin\left(\alpha^s_{0L} - \alpha^b_{0L}\right) \\ (W/\bar{U})P + \left(C_{y_r} - 1\right)R + C_{y_p} P + C_{y_\beta}\beta \end{bmatrix}$$

$$f_{12} = \frac{g}{\bar{U}} \begin{bmatrix} 0 \\ 0 \\ 0 \\ \cos\theta\cos\phi \\ \cos\theta\sin\phi \end{bmatrix}, \qquad B_1 = \begin{bmatrix} 0 & C_{l_{\delta_a}} & C_{l_{\delta_r}} \\ C_{m_{\delta_e}} & 0 & 0 \\ 0 & C_{n_{\delta_a}} & C_{n_{\delta_r}} \\ C_{z_{\delta_e}} & 0 & 0 \\ 0 & 0 & C_{y_{\delta_r}} \end{bmatrix} \qquad \text{and} \qquad f_2 = \begin{bmatrix} Q\cos\phi - R\sin\phi \\ P + Q\sin\phi\tan\theta + R\cos\phi\tan\theta \end{bmatrix}, \qquad B_2 = \begin{bmatrix} 0 & 0 & 0 \\ 0 & 0 & 0 \end{bmatrix}$$

In addition,

$$f_{1X_1}\Big|_{(X_{1_0},X_{2_0})} = f_{11X_1}\Big|_{X_{10}}$$

Hence, neglecting the $\dot{\alpha}$ stability derivatives, the linearized state transition matrix

$$A = \begin{bmatrix} C_{l_{pq}}Q_0 + C_{l_p} & C_{l_{pq}}P_0 + C_{l_{qr}}R_0 & C_{l_{qr}}Q_0 + C_{l_r} & 0 & C_{l_\beta} \\ C_{m_{pr}}R_0 - 2C_{m_{p^2}}P_0 & C_{m_q} & C_{m_{pr}}P_0 + 2C_{m_{p^2}}R_0 & C_{m_\alpha} & 0 \\ C_{n_{pq}}Q_0 + C_{n_p} & C_{n_{pq}}P_0 - C_{l_{pq}}R_0 & C_{n_r} - C_{l_{pq}}Q_0 & 0 & C_{n_\beta} \\ -V_0/\bar{U} & 1 + C_{z_q} & 0 & C_{z_\alpha} & -P_0 \\ (W_0/\bar{U}) + C_{y_p} & 0 & C_{y_r} - 1 & P_0 & C_{y_\beta} \end{bmatrix}$$

is obtained. Furthermore, the vector

$$\boldsymbol{c} = f_{11}(X_{1_0}) + f_{12}(X_{2_0}) - AX_{1_0}$$

Hence, the intercept $\boldsymbol{c}$ is calculated,

$$\boldsymbol{c} = \begin{bmatrix} -C_{l_{pq}}P_0Q_0 - C_{l_{qr}}Q_0R_0 \\ C_{m_{p^2}}(P_0^2 - R_0^2) - C_{m_{pr}}P_0R_0 + C_{m_0} - C_{m_T} \\ -C_{n_{pq}}P_0Q_0 + C_{l_{pq}}Q_0R_0 \\ \beta_0P_0 - C_{z_\alpha}\alpha_{0L}^s + C_T\sin(\alpha_{0L}^s - \alpha_{0L}^b) + (g/\bar{U})\cos\theta_0\cos\phi_0 \\ -\alpha_0P_0 + (g/\bar{U})\cos\theta_0\sin\phi_0 \end{bmatrix}$$

Note that the dynamics matrix A is determined by the X_1 component of the current state, whereas the intercept vector $\boldsymbol{c}$ is determined by the entire current state vector, including the kinematic variables in X_2. The B matrix is constant due to the linear aerodynamics hypothesis. Evidently, the slow variables dynamics are removed from consideration in the control law design process.

IV. LQ Flight Control

The flight control system block diagram is shown in Fig. 1. As can be seen, there are three command inputs: α, β, and stability axis roll rate P. They can be independently commanded or in combination. Although not shown in the diagram, there are integrators in all three command loops, not just the β loop.

A. Dynamics

The plant is augmented to include actuator dynamics, and its discrete time representation is obtained,

$$X_{k+1} = AX_k + BU_k + \boldsymbol{c}, \qquad k = 0, 1, \ldots, N-1$$

Here the state is augmented to include first-order actuator dynamics and

$$X_k = \left(P_k, Q_k, R_k, \alpha_k, \beta_k, \delta_{e_k}, \delta_{a_k}, \delta_{r_k}\right)^T \in R^8$$

The control signals are the actuator commands

$$U_k = \left(\delta_{e_{c_k}}, \delta_{a_{c_k}}, \delta_{r_{c_k}}\right)^T \in R^3$$

In the case of a loaded roll that is performed in the horizontal plane, the initial state is

$$X_0 = \left(0, Q_0, R_0, 0, \beta_0, \delta_{e_0}, \delta_{a_0}, \delta_{r_0}\right)^T$$

where the 0 subscripts of the Q and R angular rates of the aircraft and the effector deflections denote the initial trim condition, which corresponds to a steady level turn. Furthermore, a velocity vector roll maneuver will have been accomplished if the achieved terminal state is

$$X_f = \left(0, Q_0, -R_0, 0, -\beta_0, \delta_{e_0}, -\delta_{a_0}, -\delta_{r_0}\right)^T$$

Finally, the discrete-time optimization horizon N is given by

$$N = T/\Delta T$$

In this work, $\Delta T = 0.01$ s and the optimization horizon $N = 20$ so that the physical optimization horizon is $T = 0.2$ s into the future. Hence, the current pilot commands are extrapolated 0.2 s into the future.

B. Integral Action in LQ Control

Integral action is mandated by the need to reject unmodeled disturbances, as would be the case when a control surface failure occurs. Integral action is also required to accommodate subtle mismatches between the plant model and the actual plant (see, e.g., Ref. 9). Furthermore, integral action is beneficial whenever a controller that has been designed using a linearized plant model is used in a control system where the actual nonlinear plant is operational. Obviously, if the plant displays natural integral action, i.e., if the plant happens to have a pole at the origin, then in this fortunate instance there is no need to introduce integral action into the controller and, moreover, integrator windup cannot occur.

Integral action in the state space formulation requires the additional three states z_P, z_α, and z_β. The augmented state vector includes the actuator states (because first-order actuator dynamics are included in the dynamics) and integrator states (because integral action is built into the cost functional). The augmented state is

$$X_k = \left(P_k, Q_k, R_k, \alpha_k, \beta_k, \delta_{e_k}, \delta_{a_k}, \delta_{r_k}, z_{P_k}, z_{\alpha_k}, z_{\beta_k}\right)^T \in R^{11}$$

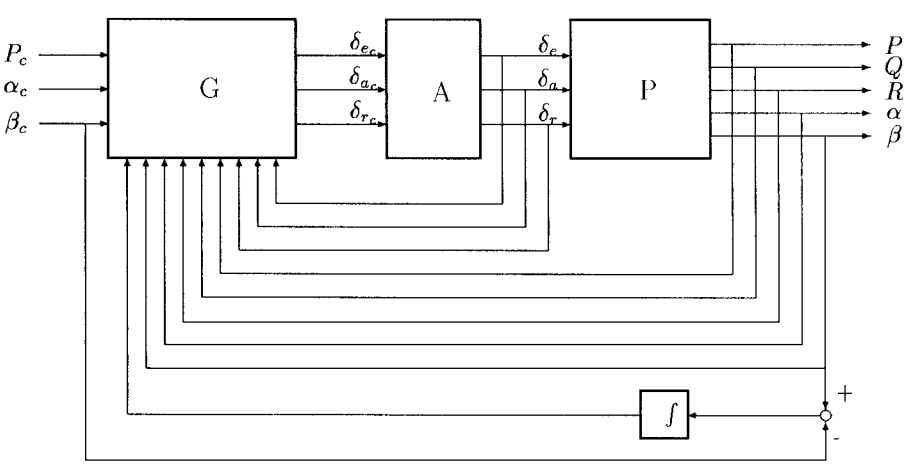

Fig. 1 Control system diagram.

The control signals are the actuator commands

$$U_k = \left(\delta_{e_{c_k}}, \delta_{a_{c_k}}, \delta_{r_{c_k}}\right)^T \in R^3$$

Define the integrator state

$$Z = \begin{bmatrix} z_P \\ z_\alpha \\ z_\beta \end{bmatrix}, \qquad Z \in R^3$$

Now

$$Z_{k+1} = Z_k + R_{k+1} - CX_{k+1}, \qquad k = 0, 1, \ldots, N-1$$

where the reference signal vector

$$\boldsymbol{R}_k = \begin{bmatrix} P_{c_k} \\ \alpha_{c_k} \\ \beta_{c_k} \end{bmatrix}, \qquad \boldsymbol{R}_k \in R^3, \qquad k = 1, 2, \ldots, N$$

The 3×8 matrix

$$C = \begin{bmatrix} 1 & 0 & 0 & 0 & 0 & 0 & 0 & 0 \\ 0 & 0 & 0 & 1 & 0 & 0 & 0 & 0 \\ 0 & 0 & 0 & 0 & 1 & 0 & 0 & 0 \end{bmatrix}$$

Obviously,

$$Z_{k+1} = Z_k + R_{k+1} - CAX_k - CBU_k - C\boldsymbol{c}$$

Hence, when integral action is included, the augmented system is obtained:

$$X_{k+1} = \boldsymbol{A}X_k + \boldsymbol{B}_1 U_k + \boldsymbol{B}_2 R_{k+1} + \boldsymbol{B}_3 c, \qquad k = 0, 1, \ldots, N-1$$

where

$$X \leftarrow \begin{bmatrix} X \\ Z \end{bmatrix} \in R^{11}, \qquad \boldsymbol{A} = \begin{bmatrix} A & 0 \\ -CA & I_3 \end{bmatrix}_{11 \times 11}$$

$$\boldsymbol{B}_1 = \begin{bmatrix} I_8 \\ -C \end{bmatrix} B, \qquad \boldsymbol{B}_2 = \begin{bmatrix} 0_{8 \times 3} \\ I_3 \end{bmatrix}, \qquad \boldsymbol{B}_3 = \begin{bmatrix} I_8 \\ -C \end{bmatrix}$$

C. Reference Signals

The reference signal $\boldsymbol{R}_k$ consists of the pilot's commands, which are input through the pitch stick, the roll stick, and the rudder pedals. Thus, for the level loaded roll, the pilot commands are

$$P_{c_1}, P_{c_2}, \ldots, P_{c_N}, \qquad \alpha_{c_1}, \alpha_{c_2}, \ldots, \alpha_{c_N} = 0$$

$$\beta_{c_1}, \beta_{c_2}, \ldots, \beta_{c_N} = 0$$

A pulse roll rate pilot command with 2.1-rad/s amplitude and 1.5-s duration is input to the roll channel flying qualities (pre)filter where a bank angle change from +72 to −72 deg is attained in about 2 s. The first-order roll flying qualities filter has a time constant of $\tau = 0.8$ to command the roll rate and a time constant of $\tau = 0.4$ to arrest the roll rate.

D. Cost Function

The regulated variables are

$$P_{c_k} - P_k, \qquad \alpha_{c_k} - \alpha_k, \qquad \beta_{c_k} - \beta_k, \qquad k = 1, 2, \ldots, N$$

The respective weights are $Q_P = 50\ \text{s}^2$, $Q_\alpha = 5000$, $Q_\beta = 21{,}000$, $Q_{I_P} = 1000$, and $Q_{I_\alpha} = Q_{I_\beta} = 1000/\text{s}^2$. In addition, the control effort is accounted for in the cost functional by penalizing the actuator deflection rates,

$$\delta_{e_{k+1}} - \delta_{e_k}, \qquad \delta_{a_{k+1}} - \delta_{a_k}, \qquad \delta_{r_{k+1}} - \delta_{r_k}$$

$$k = 0, 1, \ldots, N-1$$

and the respective weights are $R_e = 7$ and $R_a = R_r = 10^4$. Note that the elevator penalty is low to generate sufficient gain to pull the open-loop unstable pitch channel's root locus into the left-half complex plane.

To obtain good tracking of the roll rate command, the roll rate acceleration is penalized using the weight $Q_{\dot{P}} = 100\ \text{s}^4$. Furthermore, the aerodynamic angles' rates are penalized; the weights are $Q_{\dot{\alpha}} = 2 \times 10^4\ \text{s}^2$ and $Q_{\dot{\beta}} = 10^6\ \text{s}^2$. This helps to decouple the roll channel from the pitch channel and reduces the adverse yaw. Additional pitch and yaw damping action is built into the controller by also penalizing the pitch and yaw angular accelerations using the respective weights $Q_{\dot{Q}} = 8 \times 10^4\ \text{s}^4$ and $Q_{\dot{R}} = 10^5\ \text{s}^4$. Thus, in the quadratic cost, the tracking errors, including the integrals of the tracking errors, and the actuator deflection rates are penalized. In addition, when the roll stick is used, the penalties for the pitch and yaw accelerations are increased because higher damping is needed; penalties are lower otherwise. Note that these are the same penalties used for pitch and yaw commands, whose responses are not shown in this paper. Also, the penalties are the same both before and after the failure.

The optimal control signal is linear in the current state X_k and in the reference signal $\boldsymbol{R}_k$,

$$U_k = FX_k + G\boldsymbol{R}_k + \boldsymbol{h}$$

There is nothing we can do about the current state x_k. Hence, saturation avoidance is achieved by modifying the pilot-commanded reference signal, as is elucidated in the following section. The explicit formulas for the receding horizon LQ control law's matrices F and G and the vector $\boldsymbol{h}$ are given in Secs. 5 and 6 of Ref. 2.

E. Dynamic Command Limiting

High-amplitude maneuvers can induce actuator saturation. Furthermore, after an aircraft sustains damage to a control surface, its ability to produce the required control forces degrades and the controller's demands on surface deflection and rates increase, leading to actuator saturation. Obviously, advanced nonlinear controllers where actuator saturation mitigation measures are implemented are essential for actuator failure accommodation.

Actuator saturation mitigation motivates us to employ a dual-loop control structure. In the outer loop, the reference signals, namely, the pilot's commands, are modified so that the inner-loop LQ controller-generated actuator deflection commands avoid saturation. An LP optimization algorithm is used in the outer loop to obtain the required degree of relaxation of the pilot's commands. Obviously, one would like to minimize the degree of modification of the pilot's commands, while guaranteeing downstream actuator saturation avoidance. Thus, the cost functional of the LP is the weighted sum

$$J = \frac{\epsilon_P}{\|P_c\|_\infty} + \frac{\epsilon_\alpha}{\|\alpha_c\|_\infty} + \frac{\epsilon_\beta}{\|\beta_c\|_\infty}$$

where ϵ_P, ϵ_α, and ϵ_β are the absolute values of the required changes in the pilot commands. Specifically, a weighted sum of the degree of relaxation in the pilot-commanded roll rate, angle of attack, and sideslip angle is minimized by the LP module while avoiding actuator rate saturation for the elevator, ailerons, and rudder during the optimization horizon.

For example, the linear constraint equation for the elevator rate is posed as

$$\boldsymbol{g}_e < \boldsymbol{V}_{ep} \times \epsilon_p + \boldsymbol{V}_{e\alpha} \times \epsilon_\alpha + \boldsymbol{V}_{e\beta} \times \epsilon_\beta < \boldsymbol{h}_e$$

where $\boldsymbol{g}_e$ and $\boldsymbol{h}_e$ are vectors that contain the lower and upper limits of the elevator rate (± 1 rad/s). The vectors $\boldsymbol{V}_{ep}$, $\boldsymbol{V}_{e\alpha}$, and $\boldsymbol{V}_{e\beta}$ are derived from the inner-loop optimal control formulation. The relationship at the end of Sec. IV.D giving the optimal surface deflections in response to the pilot's commands is used. The optimized variables are ϵ_P, ϵ_α, and ϵ_β, the degree of relaxation of the respective P_c, α_c, and β_c pilot commands. Similar constraints are imposed for the aileron and rudder. Note that the constraints are enforced for the entire 20-step horizon.

An active set strategy that is a variation of the well-known simplex algorithm was used to solve the LP problem. The problem is posed in the canonical form

$$\min_x\{f^T\mathcal{X}\} \qquad \text{subject to: } \mathcal{A}\mathcal{X} \le b$$

Because the constraints are considered for 20 time steps into the future, reformulating the double-sided constraints for each actuator results in 120 constraints. Three more double-sided constraints are required in the formulation for ϵ_P, ϵ_α, and ϵ_β to be positive or negative, resulting in 126 total constraints. The linear program finds optimal values for ϵ_P, ϵ_α, and ϵ_β and the three additional variables, x_p, x_α, and x_β that are required to allow ϵ_P, ϵ_α, and ϵ_β to attain positive or negative values. For example, the constraint required for the change in roll command is $-\epsilon_p \le x_p \le \epsilon_p$.

V. Simulation Results

The aircraft model used in the simulations is an F-16 derivative. The open-loop plant corresponds to the flight condition: $h = 10{,}000$ ft, $M = 0.7$ ($\bar{q} = 499$ lb/ft^2), and $n = 3\,g$ ($\alpha = 6$ deg with respect to the body axis). An aircraft weighing three times the normal combat weight was trimmed in straight and level flight to obtain an AOA of 6 deg (with respect to the body x axis) and the stability and control derivatives were extracted from the database.[7] The first-order actuator dynamics are specified by the time constants $\tau_e = \tau_a = \tau_r = 0.05$ s.

At 1 s into the velocity vector roll maneuver flight, a 50% loss of rudder area is simulated. Specifically, the $C_{n_{\delta_r}}$ control derivative is reduced by 50%. Also, the $C_{y_{\delta_r}}$ and $C_{l_{\delta_r}}$ control derivatives and the C_{n_β}, C_{Y_β}, C_{n_p}, C_{n_r}, and C_{l_β} stability derivatives are modified accordingly using DATCOM.[10]

The altitude, airspeed, AOA, and sideslip angle do not change appreciably during the velocity vector roll maneuver (by design). However, the angular rates R and, in particular, P change significantly while the bank angle ϕ is slewed from $+72$ to -72 deg. The dynamics are pointwise linearized at each time step during the dynamic velocity vector roll maneuver to account for changes in the P, R, and ϕ variables.

It is important to stress that the linearization is performed about a nonsymmetrical flight condition; therefore, the resulting linear pitch and lateral/directional dynamics of the open-loop plant are strongly coupled. One of the requirements of a velocity vector roll control law is the decoupling of the closed-loop flight control system.

The response to a commanded roll rate pulse with a 2.1-rad/s amplitude and 1.5-s duration (applied to a first-order prefilter) is shown in Fig. 2. A pitch stick command of constant AOA, so that a 3-g turn is held, and a sideslip angle command of β_c, which drives the sideslip angle β from β_0 to $-\beta_0$, are shown in Fig. 3.

Specifically, we show that a velocity vector roll maneuver is indeed accomplished in ≈ 2 s. In Fig. 2 we show the good tracking of the roll rate command before and after the failure, which occurs at 1 s into the flight. The bank angle time history is shown in Fig. 4 where the new bank angle of -72 deg is intercepted at about 2 s,

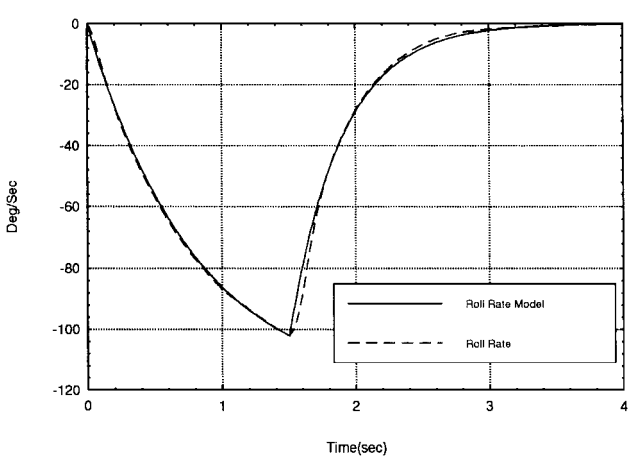

Fig. 2 Roll rate command tracking.

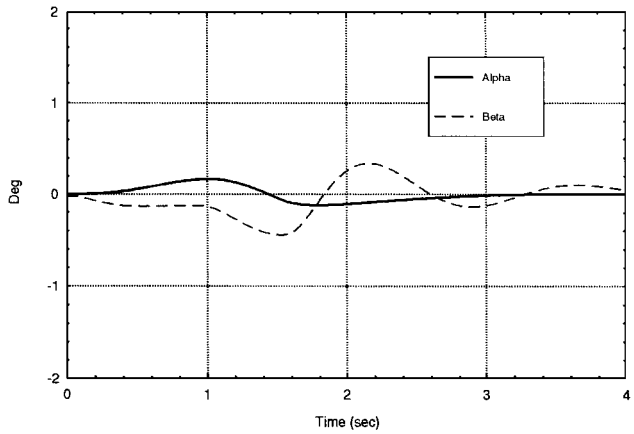

Fig. 3 Angles α and β for roll input.

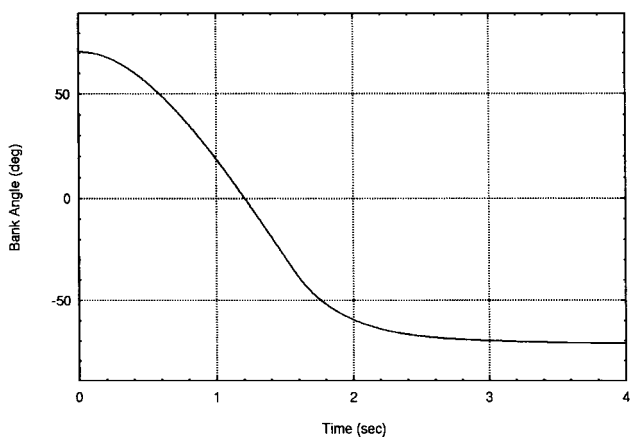

Fig. 4 Bank angle change for roll input.

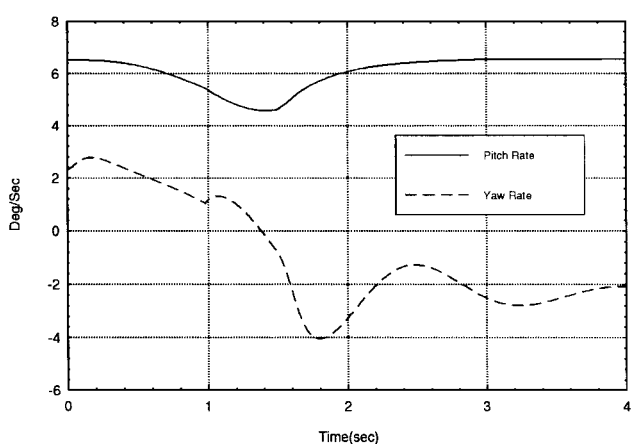

Fig. 5 Angular rates for roll input.

at which time the roll is almost arrested and $P \approx P_c \approx 0$. Figure 3 shows that during the velocity vector roll maneuver, the excursions in the aerodynamic angles are small, so that the aircraft is not unloaded. Elevator rate activity is apparent during failure onset and command reversal. In Fig. 5 the pitch rate Q and yaw rate R are shown. Because of coupling, the roll maneuver and later the failure cause fluctuation in pitch rate, but Q does return to the trim value as required. The more interesting yaw rate R does behave as expected during a velocity vector roll, and its polarity is indeed reversed, but could be better damped.

Figure 6, where the control surfaces' activity is shown, is most interesting. There are two causes for abrupt changes in actuator rate: 1) The structural change occurring in the system at the moment of failure (1 s) causes the model-driven optimization algorithm to produce a discontinuity in the commands that translates into high actuator rates, which is also determined by the actuators' deflection rate penalties. Because of coupling, a discontinuity in any of the

model's parameters will simultaneously affect all of the commands output by the optimization-based controller (according to the penalty coefficients) and cause abrupt changes in the elevator and aileron rate. 2) The abrupt change in the reference signal, which occurs at 1.5 s in the flight when the roll rate command goes out, causes a high level of actuator activity, as was also the case at time $t = 0$ when the roll rate command came in. This activity is compounded somewhat by the prediction error at this point, which assumes the pilot input is constant, but only lasts for 1 or $2\Delta t$.

In Fig. 6 it can be seen that the aileron saturates in rate (1 rad/s) at $t = 0, 1.5$ s. The LP is attenuating the roll reference model by the amount ϵ_{pi} to just satisfy the rate constraints. As can be seen, the LP is quite effective, as there are no hard limits on the actuator rates in the nonlinear simulation. As a benefit, the LP avoids the need for integrator antiwindup logic. This is because the error being integrated is between the LP-attenuated roll rate model and the actual roll rate, not between the pilot-commanded roll rate model and the actual roll rate.

In addition, a pitch pulse input of 6 deg α is given at $t = 0$ for 2 s while the aircraft is in the 3-g level turn for a total of 6 g. The tracking response compared to the α handling qualities model is shown in Fig. 7, where the sideslip is essentially zero. Note that a failure is not introduced in the simulation for Fig. 7 or the remaining plots. These plots are to demonstrate the decoupled tracking ability of the other two command inputs. Figures 8 and 9 show that there is essentially no cross coupling into the roll and yaw rates with only small elevator deflection rates.

Also, a yaw pulse input of 6 deg β is given at $t = 0$ for 2 s while the aircraft is in the 3-g level turn. The tracking response compared to the β handling qualities model is shown in Fig. 10. This is a

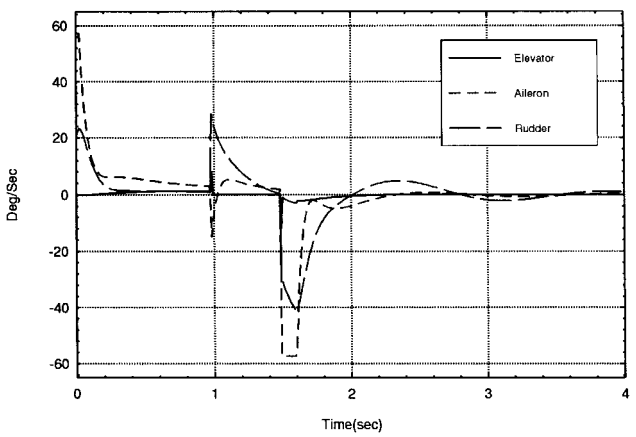

Fig. 6 Surface deflection rates.

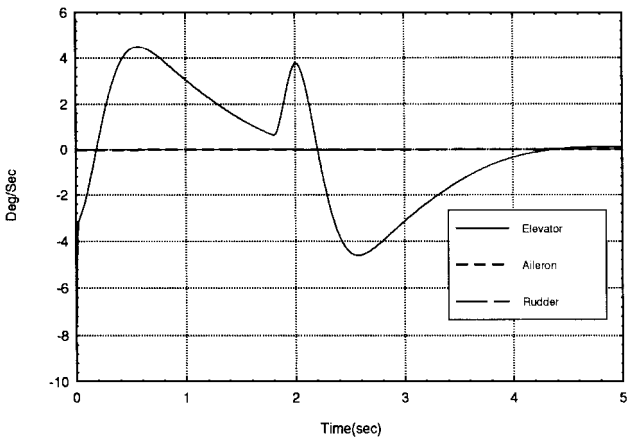

Fig. 9 Surface deflection rates.

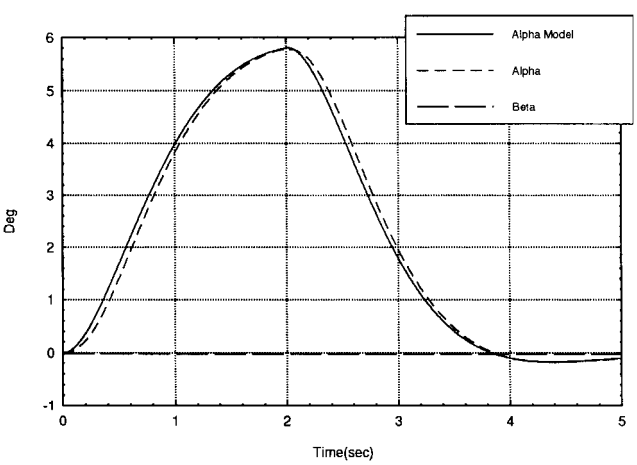

Fig. 7 Alpha command tracking.

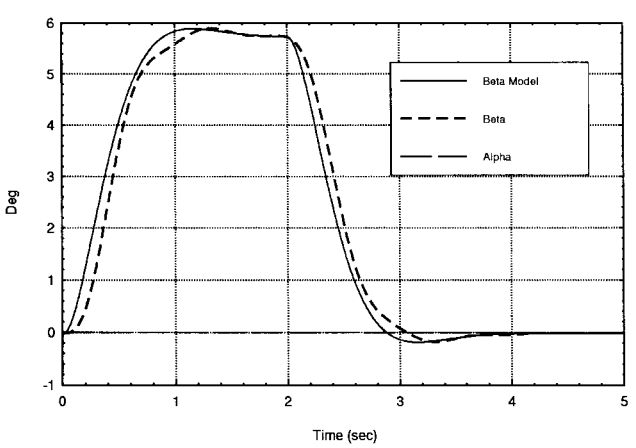

Fig. 10 Beta command tracking.

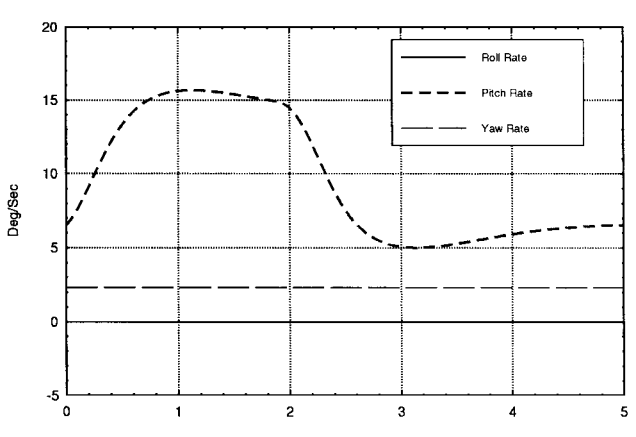

Fig. 8 Angular rates for pitch input.

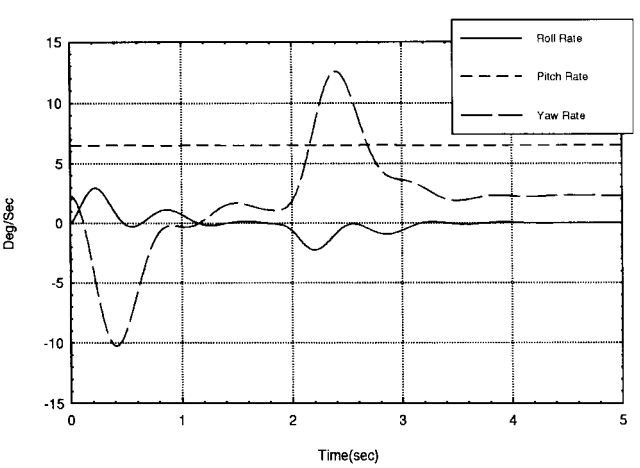

Fig. 11 Angular rates for directional input.

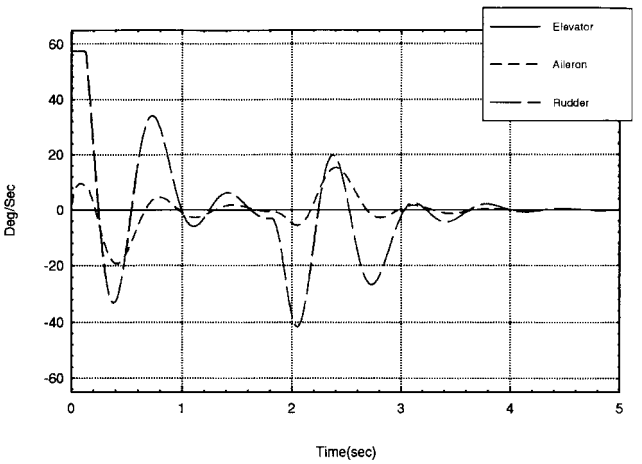

Fig. 12 Surface deflection rates.

large β input at this flight condition, but the control system holds the coupling into roll at a minimum, as can be seen in Fig. 11. The large input saturates the rudder in rate, as can be seen in Fig. 12, but the command limiting effectively modifies the β command to not exceed the rate limit; the simulation does not contain actuator rate limits.

VI. Conclusion

The nonlinear dynamics are relinearized every Δt and are assumed constant over the prediction horizon. The pointwise linearization is performed about arbitrary, nonequilibria trajectories. Also, total rather than perturbation, variables are used. The frequent relinearization guarantees the fidelity of the linear plant model used for control design and also reduces the modeling error for the on-line identification of the aerodynamic stability and control derivatives that are needed to implement an adaptive or reconfigurable control system. The plant model used for controller design does not rely on decoupled longitudinal and lateral directional channels, but rather acknowledges the coupling of the longitudinal and lateral directional dynamics introduced by the roll rate. Using a timescale separation argument, which removes the airspeed and aircraft Euler angles from consideration, allows us to settle on a five-state bare aircraft model. Furthermore, actuator constraints are included in the controller design process, mainly to enable accommodation of high-amplitude slewing commands and aerodynamic effector failures. The proposed controller has an inner-loop LQ optimization module for good small-signal tracking and an outer-loop LP optimization module for modifying the pilot reference signals to avoid actuator rate saturation during high-amplitude maneuvers. Although bounded input bounded output (BIBO) stability is not guaranteed, good tracking performance is achieved. The performance of the nonlinear flight control system is demonstrated for an aggressive velocity vector roll maneuver with a 50% loss of rudder area during the 3-*g* loaded roll maneuver. Large pitch and yaw input command responses with no failures are also shown. The nonlinear, on-line designed feedback controller maintains axes decoupling for a rudder failure during the 3-*g* loaded roll maneuver, thus significantly alleviating the pilot's workload.

Acknowledgment

This paper was presented at the 1997 American Control Conference, Albuquerque, New Mexico, June 4–6, 1997.

References

[1]Pachter, M., Chandler, P. R., and Mears, M., "Modeling and Control of Velocity Vector Rolls," *Proceedings of the AIAA Guidance, Navigation, and Control Conference*, AIAA, Washington, DC, 1995, pp. 20–37 (AIAA Paper 95-3177, Aug. 1995).

[2]Pachter, M., and Chandler, P. R., "Velocity Vector Roll Control," AIAA Paper 96-3867, Aug. 1996.

[3]Boyum, K. E., Pachter, M., and Houpis, C. H., "High Angle of Attack Velocity Vector Rolls," *Control Engineering Practice*, Vol. 3, No. 8, 1995, pp. 1087–1093.

[4]Pachter, M., Chandler, P. R., and Mears, M., "Reconfigurable Tracking Control with Saturation," *Journal of Guidance, Control, and Dynamics*, Vol. 18, No. 5, 1995, pp. 1016–1022.

[5]Smith, L., Chandler, P., and Pachter, M., "Regularization Techniques for Real-Time Identification of Aircraft Parameters," *Proceedings of the AIAA Guidance, Navigation, and Control Conference* (New Orleans, LA), AIAA, Reston, VA, 1997, pp. 1466–1480 (AIAA Paper 97-3740).

[6]Stevens, B. L., and Lewis, F. L., *Aircraft Control and Simulation*, Wiley, New York, 1992, p. 141.

[7]"Simulation/Rapid-Prototyping Facility," Century Computing, Inc., Sun/Unix version, Dayton, OH, Oct. 1992.

[8]Blakelock, J. H., *Automatic Control of Aircraft and Missiles*, 2nd ed., Wiley, New York, 1991.

[9]Pachter, M., D'Azzo, J. J., and Veth, M., "Proportional and Integral Control of Nonlinear Systems," *International Journal of Control*, Vol. 64, No. 4, 1996, pp. 679–692.

[10]Hoak, D. E., and Fink, R. D., "USAF Stability and Control Digital DATCOM," U.S. Air Force Flight Dynamics Lab., AFFDL-TR-79-3032, Wright–Patterson AFB, OH, April 1979.